Trans Indian Inst Met (2022) 75(11):2875–2882
https://doi.org/10.1007/s12666-022-02670-x

ORIGINAL ARTICLE

Heat Treatment Behavior, Microstructure and Mechanical Properties of TiO_2@CNTs/7075 Al Composites Fabricated by Ultrasonic-Assisted Casting

Xiuliang Zou[1,2] · Hong Yan[1,2] · Kai Zhibin Junjie TuLiuXiong[1,2,1,2,1,2]

Received: 5 January 2022 / Accepted: 13 June 2022 / Published online: 8 July 2022

Abstract The carbon nanotubes coated with TiO_2 reinforced 7075 Al composites were fabricated by ultrasonic-assisted casting in this study. The heat treatment behavior, microstructure and mechanical properties of TiO_2@CNTs/7075 Al composites were investigated by X-ray diffraction (XRD), scanning electron microscopy (SEM), energy dispersive X-ray spectrometry (EDS), transmission electron microscope (TEM), tensile and hardness tests. The experimental results reveal that CNTs accelerate the precipitation process of the TiO_2@CNTs/7075 Al composites owing to the formation of dislocations caused by TiO_2@CNTs. 7075 Al alloy reaches the peak aging time at 24 h with the hardness of 152.3 HV, while TiO_2@CNTs/7075 Al composites reach the peak aging time at 18 h with the hardness of 171.1 HV. Meanwhile, the aging strengthening effect of the TiO_2@CNTs/7075 Al composites is less significant than that of matrix alloy, due to the introduction of TiO_2@CNTs leading to a significant reduction and an uneven distribution of the precipitations.

Keywords TiO_2@CNTs · Heat treatment behavior · Microstructure · Mechanical properties · Precipitation process · Aging strengthening effect

1 Introduction

Because of their excellent performance such as high specific strength, specific stiffness, specific modulus and low linear expansion coefficient, aluminum matrix composites are extensively used in military, aerospace and automobile industries [1, 2]. Thus, more attention has been attracted to the aluminum matrix composites as an emerging material in recent years. And, carbon nanotubes (CNTs) have been developed as an ideal reinforcement for aluminum matrix composites because of extraordinary high mechanical properties, admirable thermal and electrical conductivity [3]. Nowadays, multiple methods, such as casting [4], powder metallurgy [5] and friction stir process [6], have successfully fabricated CNTs reinforced aluminum matrix (CNTs/Al) composites. Nevertheless, the application of CNTs/Al composites fabricated by above methods is still greatly restricted by some problems such as easy agglomeration of CNTs, poor interface bonding and wettability between CNTs and Al and uncontrollability of CNTs/Al interfacial reaction [7].

Accordingly, CNTs/Al composites fabricated by various methods need to be post-treated to further improve their mechanical properties. Kwon et al. [8] fabricated CNTs/Al composites by the method of spark plasma sintering and subsequent hot extrusion. They indicated that the hot extrusion process contributed to further improve dispersity, density and orientation of CNT and achieved good interface bonding between CNTs and Al. Kai et al. [9] designed a route combining powder metallurgy with hot extrusion to fabricate CNT/7055 Al composites. They found that the higher temperature extrusion contributed to the CNT orientation along the extrusion direction, which was beneficial to increase the ultimate tensile strength of the materials. As can be seen from the above, most of the present investigations concentrated on the hot extrusion for the post-treatment of CNTs/Al

✉ Hong Yan
hyan@ncu.edu.cn

[1] School of Mechanical and Electrical Engineering, Nanchang University, Nanchang 330031, China

[2] Key Laboratory of Light Alloy Preparation & Processing in Nanchang City, Nanchang 330031, China

composites, which aimed to further improve the dispersion and orientation of CNTs as well as interface bonding between CNTs and Al. It is well known that 7075 Al alloy is a typically heat treatable Al–Zn–Mg–Cu alloy. Some defects such as segregation rising from forming process will result in a rupture ahead of materials under external load. And, heat treatment is a common process to improve the strength of materials after the forming process. Accordingly, it is necessary to carry out the heat treatment process for the CNTs/7075 Al composites. However, there are only a few studies about the effect of heat treatment on CNTs/Al composites [10], especially for CNTs/7075 Al composites. Moreover, the influence of different reinforcements on the heat treatment behavior of aluminum matrix composites is obviously not clear, though some scholars have studied the effects of the reinforcements on the heat behavior of aluminum matrix composites. Li et al. [11] studied the influence of the TiN nanoparticles addition on the heat behavior of the Al–Zn–Mg–Cu alloy. They found that the TiN nanoparticles promoted the dissolution of alloy elements and restrained the fine grains during solution heat treatment process. Besides, the TiN nanoparticles accelerated the process of the supersaturated solid solution evolving into to the G.P. zones, but restrained the precipitated phase. Xu et al. [12] investigated the effect of Ag additions on the precipitation of 7075 Al alloy. They concluded that a small amount of Ag addition significantly accelerated the precipitation in 7075 Al alloy, decreasing obviously the peak aging time, due to the formation of Mg–Ag clusters. It is of great importance to make it clear that the influence of reinforcements on the heat treatment behavior of aluminum matrix composites contribute to exert excellent strengthening effect of reinforcements. Nevertheless, investigations on the influence of CNTs addition on the heat behavior of the CNTs/7075 Al composites have been little reported.

This present work aimed to study the influence of heat treatment on the microstructure and mechanical properties of TiO_2@CNTs/7075 Al composites. In addition, the influence of CNTs addition on the heat behavior of TiO_2@CNTs/7075 Al composites was analyzed. This study has an important guiding function for developing the high performance CNTs/Al composites.

2 Materials and Methods

The commercial 7075 Al alloy was employed as the matrix material in this experiment. And, the chemical composition of 7075 Al alloy is shown in Table 1. The as-received CNTs with an outer diameter of 30 ~ 80 nm and a length of several microns were used as the reinforcements, which were supplied by Chengdu organic chemistry co., Lt, Chinese academy of sciences.

In order to improve the wettability between Al and CNTs, the surface modification method of electroless plating was used to coat a layer of TiO_2 particles on the surface of CNTs. And, the Al–TiO_2@CNTs intermediate block was prepared by the method of ball milling and cold compacting. Then, the Al–TiO_2@CNTs intermediate block was added into the 7075 Al alloy melt with the assistance of high-energy ultrasonic vibration. Finally, the as-cast 0.9 wt.% TiO_2@CNTs/7075 Al composites were successful fabricated. According to our early research group, the performance of 0.9 wt.% TiO_2@CNTs addition of CNTs/Al composites was better. The billets were machined into cylindrical metal sheets with the diameter of 10 mm and the height was 10 mm. Firstly, the TiO_2@CNTs/7075 Al composites were solution-treated at 480 °C for 4 h, and then quenched in water as soon as possible, finally aged at 120 °C from 6 to 24 h. The specific heat treatment scheme is presented in Table 2.

The microstructure and fracture surfaces were observed by SEM (Tescan-Vega3). The element distribution was detected by EDS (Tescan-Vega3). XRD (Rigaku) was employed to detect material composition. TEM (TalosF200X) was employed to observe the CNTs and precipitation. The Vickers hardness of the samples was measured on a HV-1000 microhardness tester applying a load of 300 g for 10 s. The hardness values of each sample were calculated by averaging seven test results in order to eliminate the random error. The tensile samples under different conditions were processed into tensile bars, for which the gauge length was 45 mm and the diameter was 9 mm, according to the national standard GB/T 228–2002. The tensile tests were carried out by an UTM5105 tensile tester at a strain rate of 0.001 s^{-1}. In order to ensure the reliability of measured results, at least three samples were tested for each condition.

Table 2 The heat treatment process scheme

No	Heat treatment scheme
1	(480 °C,4 h) + water quench (25 ± 5 °C)
2	(480 °C,4 h) + water quench (25 ± 5 °C) + (120 °C,6 h)
3	(480 °C,4 h) + water quench (25 ± 5 °C) + (120 °C,12 h)
4	(480 °C,4 h) + water quench (25 ± 5 °C) + (120 °C,18 h)
5	(480 °C,4 h) + water quench (25 ± 5 °C) + (120 °C,24 h)

Table 1 Chemical composite of 7075 Al alloy in wt.%

Element	Zn	Mg	Cu	Mn	Ti	Cr	Si	Fe	Al
wt.%	5.23	2.1	1.45	0.3	0.16	0.23	0.22	0.22	Bal

3 Results and Discussion

3.1 Microstructure of TiO_2@CNTs/7075 Al Composites

The SEM micrographs and EDS analysis results of TiO_2@CNTs/7075 Al composites are displayed in Fig. 1. As can be observed from Fig. 1a, the microstructure of the TiO_2@CNTs/7075 Al composites consists of α-Al matrix, grain boundary eutectic phases and black phase. Also, it can be observed that eutectic structure consists of bright lamellar phase, black line-shaped phase and gray block-shaped phase, as illustrated in Fig. 1b and c showing eutectic structure at high magnification. The EDS analysis result of bright lamellar phase displayed in Fig. 1d indicates that its stoichiometry is 60.22 at.% Al, 5.89 at.% Zn, 5.89 at.% Mg, and 3.84 at.% Cu. This is due to the reason that Cu and Al atoms have dissolved back into the $MgZn_2$ phase and formed the $Mg(Zn,Cu,Al)_2$ phase whose crystallographic lattice constant is identical to the $MgZn_2$ phase. As exhibited in Fig. 1e, the EDS result of gray block-shaped phase indicates that its stoichiometry is 85.02 at.% Al, 1.73 at.% Zn, 1.55 at.% Mg, 5.20 at.% Cu, 3.66 at.% Fe, corresponding to the stoichiometry of the Al_7Cu_2Fe phase. As depicted in Fig. 1f, the EDS result of black line-shaped phase reveals that its stoichiometry is 6.81 at.% Mg, 4.84 at.% Si, corresponding to the stoichiometry of Mg_2Si phase. In addition, the element surface scanning analysis of TiO_2@CNTs/7075 Al composites is conducted, as displayed in Fig. 2. The result shows that Ti, C, and O elements are concentrated in the black phase, proving that the black phase is the TiO_2@CNTs. Therefore, the as-cast TiO_2@CNTs/7075 Al composites consist mainly of α-Al, TiO_2@CNTs, $Mg(Zn,Cu,Al)_2$, Al_7Cu_2Fe and Mg_2Si phases.

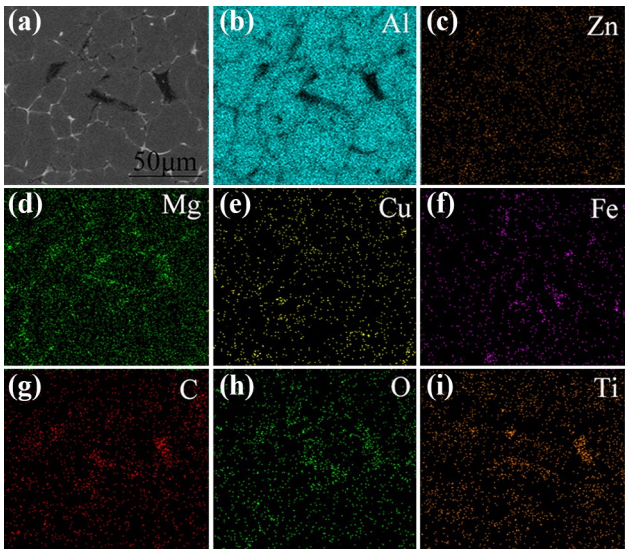

Fig. 2 Element surface scanning analysis of TiO_2@CNTs/7075 Al composites **a** SEM image **b-i** corresponding element distribution

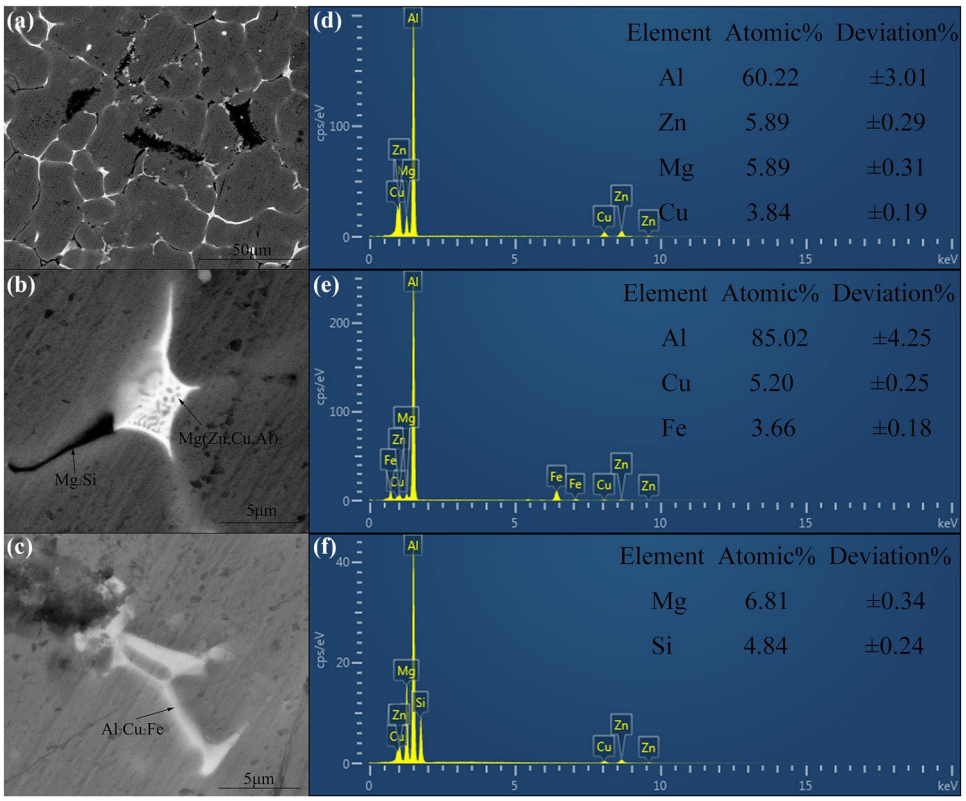

Fig. 1 SEM micrographs and EDS analysis results of TiO_2@CNTs/7075 Al composites **a** micrograph of the composites at low magnification **b-c** micrograph of eutectic structure at higher magnification **d** EDS result of bright lamellar structure **e** EDS result of gray block phase **f** EDS result of black line phase

3.2 Effect of Heat Treatment on Microstructure

The SEM micrographs and EDS analysis result of TiO_2@CNTs/7075 Al composites under different heat treatments are depicted in Fig. 3. As can be noted from Fig. 3a, the second phases at the grain boundaries evolve into discontinuous phases after solution heat treatment. In addition, the bright lamellar phases disappear while only insoluble phases are left. This is because the $Mg(Zn,Cu,Al)_2$ phase with low melting point gradually dissolves back into α-Al matrix, which results in a reduction of the second phases segregating at the grain boundaries. The EDS result of gray block-shaped phase presented in Fig. 3c indicates that its stoichiometry is 83.31 at.% Al, 1.15 at.% Zn, 1.82 at.% Mg, 6.04 at.% Cu, 4.69 at.% Fe, closing to the stoichiometry of Al_7Cu_2Fe phase. Because of its high melting point, no change in the Al_7Cu_2Fe phase occurs though the materials are solution-treated at 480 °C for 4 h. A number of coarse black phases are formed during solution heat treatment process. The EDS result of coarse black phase exhibited in Fig. 3d reveals that its stoichiometry is 5.64 at.% Mg, 3.49 at.% Si, closing to the stoichiometry of Mg_2Si phase. According to our previous study [13], the diffusion coefficients of Cu and Zn are faster than those of Si and Mg in Al(s). Zn and Cu elements can easily go into solid solution with Al matrix, while Mg and Si elements segregate at dislocations caused by CNTs and form coarse Mg_2Si phase [10]. Besides, the EDS result of black phase depicted in Fig. 3e shows that its stoichiometry is 84.64 at.% C, 6.14 at.% O, 5.58 at.% Al, 0.05 at.% Ti, which is confirmed as TiO_2@CNTs.

The aging heat treatment was carried out to re-precipitate the solute elements, following the solution heat treatment. The SEM micrograph of TiO_2@CNTs/7075 Al composites at 120 °C aged for 18 h is illustrated in Fig. 3b, after solution heat treatment at 480 °C for 4 h. It can be noted that the microstructure of the T6-treated composites almost exhibits no change, compared to the solution-treated composites, which is limited by the resolution of SEM. According to previous study [14], the size of aging precipitation in 7075 aluminum matrix composites is nanoscale, whose results in the precipitations can not be observed using SEM.

Figure 4 is the TEM morphology of TiO_2@CNTs/7075 Al composites under T6 heat treatment. It can be noted that the $MgZn_2$ phases precipitate at the interface between CNTs and Al, as depicted in Fig. 4a. In addition, the precipitate-free zones (PFZ) are observed around CNTs, as shown in Fig. 4b, which is consistent with the study of Zhao et al. [10]. It was reported [15] that the precipitations preferred to nucleate at the defects such as grain boundaries and dislocations during the aging process. It is well known that the difference of the thermal expansion coefficient between Al and CNTs would lead to the formation of dislocations, where the thermal expansion coefficient of CNTs and Al are 0.7×10^{-6}/k and 25.9×10^{-6}/k, respectively [16]. Thus, a number of dislocations are easy to be formed at the interface between Al and CNTs, as shown in Fig. 4c. Therefore, $MgZn_2$ phases precipitating at the interface between CNTs and Al are observed. Moreover, the $MgZn_2$ phases tend to precipitate around CNTs, which result in an uneven distribution of the

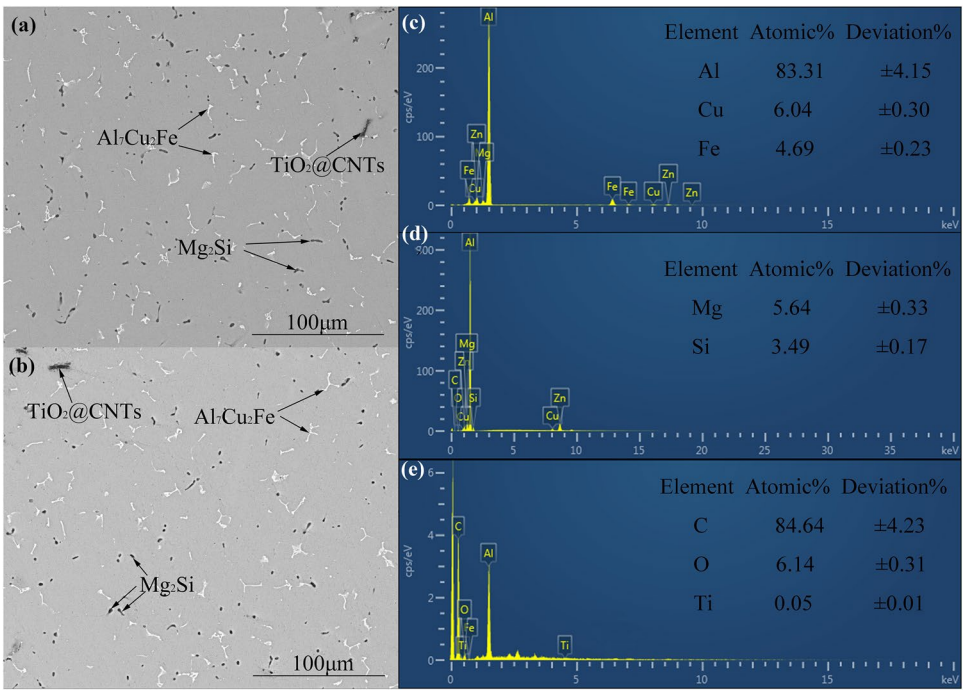

Fig. 3 SEM micrograph and corresponding EDS spectra of TiO_2@CNTs/7075 Al composites under different heat treatment **a** SEM micrograph under solution heat treatment **b** SEM micrograph under T6 heat treatment **c** EDS result of gray block phase **d** EDS result of coarse black phase **e** EDS result of black phase

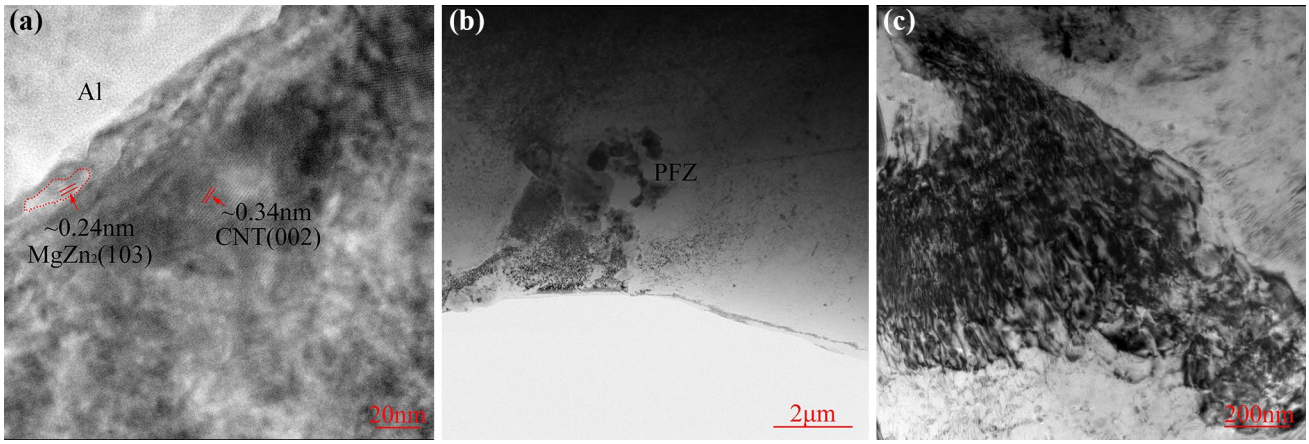

Fig. 4 TEM images of TiO_2@CNTs/7075 Al composites after T6 heat treatment **a** HRTEM image **b** precipitation-free zones (PFZ) **c** dislocations image

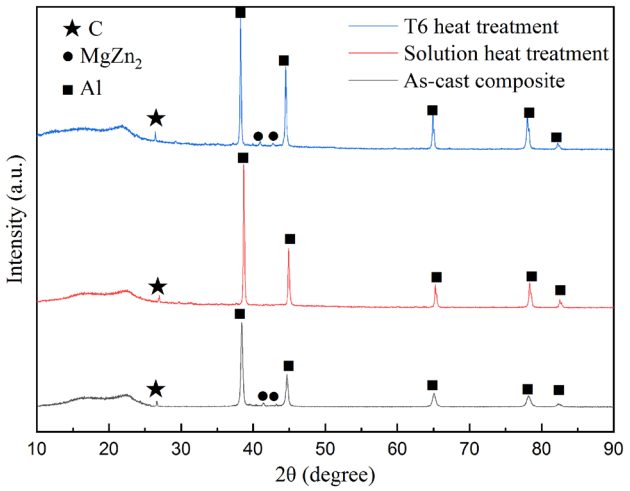

Fig. 5 XRD patterns of TiO_2@CNTs/7075 Al composites under different heat treatment

precipitations. Accordingly, the precipitate-free zones are formed around CNTs, which is adverse to the mechanical properties of the materials.

Figure 5 is the XRD patterns of TiO_2@CNTs/7075 Al composites under different heat treatments. The C peak can be found in all XRD patterns, which further proves that CNTs have been successfully added into 7075 Al alloy. But TiO_2 peak can not be observed in all XRD patterns, due to low content. Also, the $MgZn_2$ peak can be found in the XRD patterns of the TiO_2@CNTs/7075 Al composites with and without T6 heat treatment, which indicates $MgZn_2$ phase dissolving into matrix after solution heat treatment and re-precipitating followed by aging heat treatment.

3.3 Effect of Heat Treatment on Mechanical Properties

The hardness values of 7075 Al alloy and TiO_2@CNTs/7075 Al composites aged at 120 °C for different times after solution heat treatment at 480 °C for 4 h are depicted in Fig. 6a. As can be observed, the hardness of TiO_2@CNTs/7075 Al composites rises with increasing aging time and then reaches the peak, while begins to decrease with the aging time continuing to increase. The similar phenomenon is observed in 7075 Al alloy. The hardness of 7075 Al alloy reaches the peak value of 152.3 HV when aging time reaches 24 h. While TiO_2@CNTs/7075 Al composites aged at 18 h reach the peak value with the hardness of 171.1 HV. It can be noted that the peak aging time of TiO_2@CNTs/7075 Al composites is significantly earlier than that of 7075 Al alloy. The introduction of CNTs can accelerate the precipitation process of the 7075 Al alloy because of the formation of dislocations caused by CNTs. This is because the dislocations serve as channels for element diffusion, which contributes to accelerate the precipitation process [17].

The hardness values of 7075 Al alloy and TiO_2@CNTs/7075 Al composites under different heat treatments are displayed in Fig. 6b. Compared to the 7075 Al alloy, the hardness of TiO_2@CNTs/7075 Al composites reaches 126 HV, increasing by 32.22%. This is owing to the comprehensive strengthening of multi-mechanisms such as grain refinement strengthening, dislocation strengthening, load transfer strengthening and Orowan strengthening. The hardness of the composites reaches 163.8 HV after solution heat treatment, a 30% improvement in the as-cast composites, due to the Zn and Cu elements dissolving into Al matrix and forming supersaturated solid solution. While the hardness of the T6-treated composites is 171.1 HV, only showing a minor improvement, compared to the solution-treated composites. This insignificant effect is shown in two aspects.

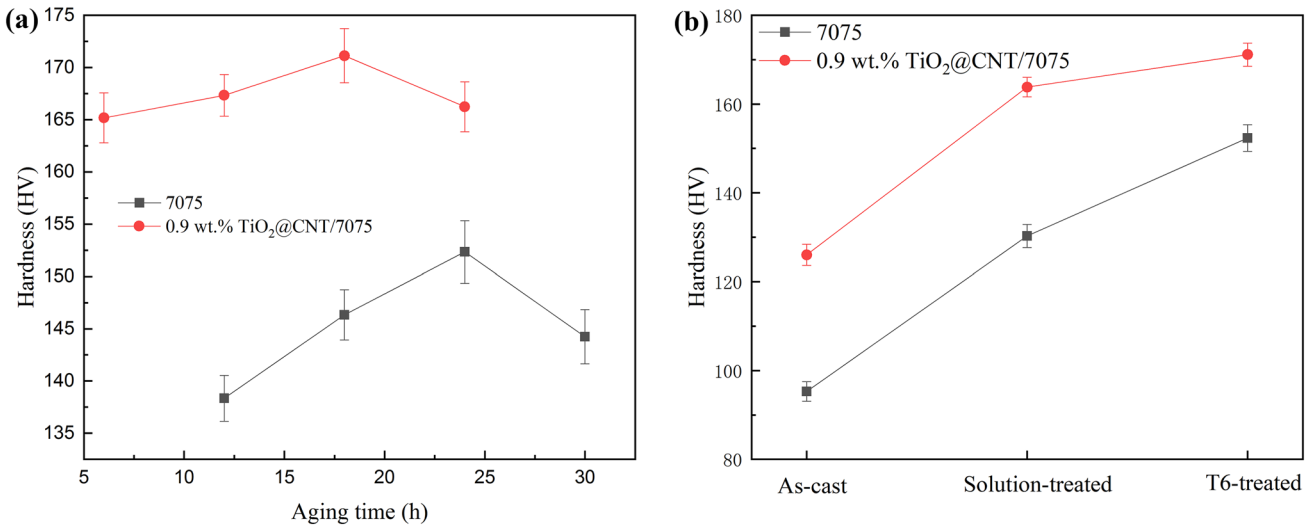

Fig. 6 Hardness values of 7075 Al alloy and TiO_2@CNTs/7075 Al composites **a** aging-treated at 120 °C for different time **b** under different heat treatment

Firstly, coarse Mg_2Si phase is formed during solution heat treatment, which results in the Mg element being consumed. Thus, Mg element can not engage the subsequent aging heat process, which leads to a reduction of the $MgZn_2$ precipitations. Secondly, the introduction of CNTs results in an uneven distribution of the precipitations.

Figure 7 is the mechanical properties of 7075 Al alloy and TiO_2@CNTs/7075 Al composites under different heat treatments. As can be observed, the mechanical properties of TiO_2@CNTs/7075 Al composites exhibit a significant improvement after solution heat treatment, where the yield strength, ultimate tensile strength and elongation of the composites are significantly increased from 201.2 MPa, 261.7 MPa and 1.6% to 262.4 MPa, 338.1 MPa and 3.5%, respectively, compared to the as-cast TiO_2@CNTs/7075 Al composites. While the yield strength and ultimate tensile strength of the T6-treated composites are 298.9 MPa and 379.7 MPa, respectively, only increasing by 36.5 MPa and 41.6 MPa, respectively, which is in accordance with the hardness tests trends. However, the elongation of the sample is only 2.7% after aging heat treatment, decreasing by 22.9%. This is because the precipitations hinder dislocation motion, which decreases the plasticity of the materials.

The fractographs of TiO_2@CNTs/7075 Al composites after different heat treatments are characterized in Fig. 8. As depicted in Fig. 8a, it can be found that the fractograph of the solution-treated composites indicates predominantly quasi-cleavage rupture, in which ductile dimples and tearing

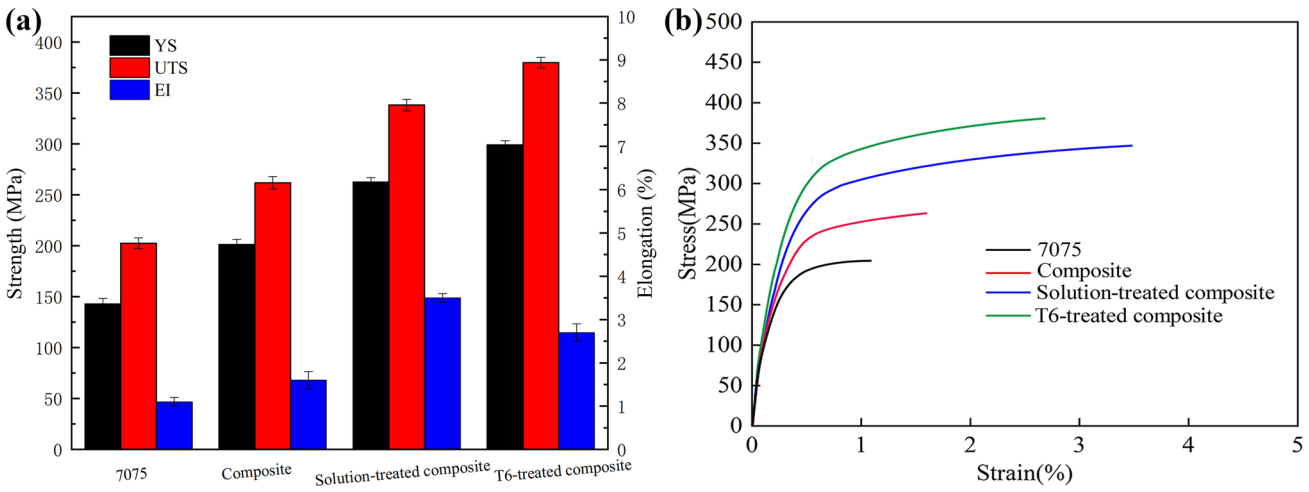

Fig. 7 Mechanical properties of 7075 Al alloy and TiO_2@CNTs/7075 Al composites under different heat treatment **a** Histogram statistics **b** Stress–strain curve

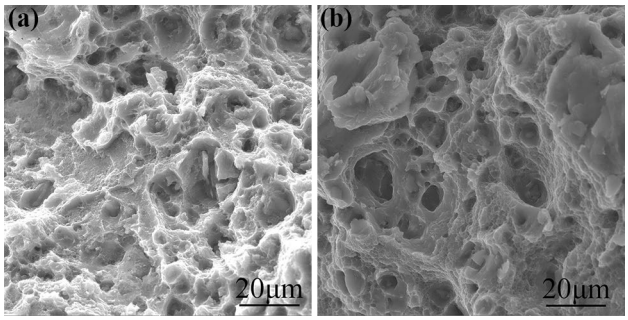

Fig. 8 SEM morphology of the fracture surfaces of TiO_2@CNTs/7075 Al composites under different heat processes **a** solution-treated (480 °C/4 h) **b** T6-treated (480 °C/4 h + 120 °C/18 h)

ridges are observed obviously. This is due to the reason that the second phases at grain boundaries are dissolved back into matrix, which significantly improves mechanical properties of the samples under solution heat treatment. The fracture surface of the T6-treated composites also indicates predominantly quasi-cleavage rupture, as displayed in Fig. 8b, while only a few tearing ridges are observed, which is in accordance with their lower plasticity.

3.4 Strengthening Mechanism

The solute elements at the grain boundaries are dissolved into matrix after solution treatment, resulting in the lattice distortion and hindering the dislocation motion, which contributes to an improvement in the yield strength of the materials. The solid solution strengthening can be expressed by the Fleischer equation [18]:

$$\Delta\sigma_{ss} = MGb\varepsilon_{ss}^{\frac{3}{2}}c^{\frac{1}{2}} \tag{1}$$

where M denotes the orientation factor (3.06 for the fcc), G represents the shear modulus (26.9 GPa), b is the Burgers vector (0.286 nm), ε_{ss} is the lattice strain and c is the solute concentration. The differences in atomic radii between solute and solvent cause the lattice strain. For quantitative calculation, it has been assumed that Zn, Mg and Cu elements are all dissolved into the matrix and the effects of different solute elements can be additive. The contributions to the yield strength from Zn, Mg and Cu atoms are 2.9 MPa (wt.%$^{-1}$), 18.6 MPa (wt.%$^{-1}$) and 13.8 MPa (wt.%$^{-1}$), respectively [18]. Therefore, $\Delta\sigma_{ss}$ is estimated to be ~ 74.2 MPa.

The precipitations interacting with dislocations hinder their motion, leading to an increase of the strength of the composites. The precipitation strengthening can be give (2)

$$\Delta\sigma_{ps} = M\frac{0.4Gb}{\pi\sqrt{1-\upsilon}}\frac{\ln(2\bar{r}/b)}{\lambda_p} \tag{2}$$

$$\bar{r} = \sqrt{\frac{2}{3r}} \tag{3}$$

where υ is the Poisson ratio (0.33), r denotes the average circular cross-sectional radius of the spherical precipitate, r and λ_p represent the average radius and spacing of the precipitations, respectively. According to TEM result of the precipitation and early study [18], the values of r and λ_p are 16 nm and 35 nm, respectively. So, $\Delta\sigma_{ps}$ is estimated to be ~ 93.1 MPa.

It can be seen that the difference between experimental and theoretical values for $\Delta\sigma_{ss}$ is small, because Zn Mg and Cu elements are not all in solid solution in the T6-treated condition due to forming the precipitates at the grain boundaries. While the difference between experimental and theoretical values for $\Delta\sigma_{ps}$ is large, due to a significant reduction and an uneven distribution of the precipitations caused by the introduction of CNTs.

4 Conclusions

1. TiO_2@CNTs/7075 Al composites at 18 h reach peak value with the hardness of 171.1 HV, while 7075Al alloy at 24 h reaches the peak value with the hardness of 152.3 HV, during the aging heat treatment process. It suggests that CNTs accelerate the precipitation process of the TiO_2@CNTs/7075 Al composites, due to the formation of dislocations caused by CNTs.

2. The strength and hardness of the TiO_2@CNTs/7075 Al composites exhibit a significant improvement under solution heat treatment, where the hardness, yield strength and ultimate tensile strength are increased from 126.0 HV, 201.2 MPa and 261.7 MPa to 163.8 HV, 262.4 MPa and 338.1 MPa, respectively, compared to the as-cast composites.

3. The weakening of the aging strengthening of the TiO_2@CNTs/7075 Al composites is observed, due to a significant reduction and an uneven distribution of the precipitations caused by the introduction of CNTs. Compared to the solution-treated composites, the hardness, yield strength and ultimate tensile strength of the T6-treated composites are 171.1 HV, 298.9 MPa and 379.7 MPa, respectively, only increasing by 7.3 HV, 36.5 MPa and 41.6 MPa, respectively.

Acknowledgements The authors express their gratitude to the National Natural Science Foundation of China (51965040).

References

1. Chen X H, and Yan H, *Mater Des* **94** (2016) 148.
2. Swarndeep S, Rupinder S, and Simranpreet S G, *Trans Indian Inst of Met* **72** (2019) 181.

3. Zhou W W, Yamamoto G, Fan Y C, Kwon H, Hashida T, and Kawasaki A, *Carbon* **106** (2016) 37.
4. Wu Q J, and Yan H, *Metall Mater Trans A* **49** (2018) 2363.
5. Trinh P V, Luan N V, Phuong D D, Minh P N, Weibel A, Mesguich D, and Laurent C, *Composites Part A* **105** (2018) 126.
6. Hosseini S A, Ranjbar K, Dehmolaei R, and Amirani A R, *J Alloys Compd* **622** (2015) 725.
7. Zhang X, Li S F, Pan B, Pan D, Liu L, Hou X D, Chu M Q, Kondoh K and Zhao M Q, *Carbon* **155** (2019) 686.
8. Kwon H, Estili M, Takagi K, Miyazaki T, and Kawasaki A, *Carbon* **47** (2018) 570.
9. Kai M, Liu Z Y, Zhang X X, Xiao B L, and Ma Z Y, Sci China Technol Sci **64** (2021) 1.
10. Zhao K, Liu Z Y, Xiao B L, Ni D R, and Ma Z Y, *Acta Metall Sin (Engl Lett)* **31** (2018) 134.
11. Li X W, Cai Q Z, Zhao B Y, Liu B, and Li W W, *J Alloys Compd* **746** (2018) 462.
12. Xu X F, Zhao Y G, Wang X D, Zhang Y Y, and Ning Y H, *Mater Sci Eng A* **648** (2015) 367.
13. Zou X L, Yan H, and Chen X H, Trans Nonferrous Met Soc China **27** (2017) 2146.
14. Zhang P X, Yan H, Liu W, Zou X L, and Tang B B, *Metals* **9** (2019) 44.
15. Ji H, Peng X, Zhang X L, Liu W C, Wu G H, Zhang L, and Ding W J, *J Alloys Compd* **791** (2019) 655.
16. Guo B S, Zhang X M, Cen X, Chen B, Wang X H, Song M, Ni S, Yi J H, Shen T, and Du Y, *Carbon* **139** (2018) 459.
17. Chen L, Yuan S W, Kong D M, Zhao G Q, He Y Y, and Zhang C S, *Mater Des* **182** (2019) 107999.
18. Ma K K, Wen H M, Hu T, Topping T D, Isheim D, Seidman D N, Lavernia E J, and Schoenung J M, *Acta Mater* **62** (2014) 141.